Chiroptical properties of cyanine aggregates: hierarchical modelling from monomers to bundles†

Francesco Bertocchi[a‡], Shahana Nizar[b‡], Cristina Sissa[a], Minghao Li[c], Thomas W. Ebbesen[b], Cyriaque Genet[b*], Anna Painelli[a*]

[a] *Dipartimento di Scienze Chimiche, della Vita e della Sostenibilità Ambientale, Università di Parma, Parco Area delle Scienze 17A, 43124, Parma, Italy*
[b] *CNRS, CESQ-ISIS University of Strasbourg UMR 7006, F-67000 Strasbourg, France*
[c] *Quantum Sensing Laboratory Department of Physics University of Basel, Switzerland*
[‡] *Equally contributing authors*

Email: genet@unistra.fr, anna.painelli@unipr.it

1 Rotational strengths and sum rule

The sum of the rotational strengths on all the excited states is:

$$\sum_f R_{gf} = \sum_f \mathrm{Im}(\langle g|\,\hat{\vec{\mu}}\,|f\rangle \cdot \langle f|\,\hat{\vec{m}}\,|g\rangle) = \mathrm{Im}(\langle g|\,\hat{\vec{\mu}} \sum_f |f\rangle\,\langle f|\,\hat{\vec{m}}\,|g\rangle)$$

where Im(.) takes the imaginary part of the term in parenthesis, $|g\rangle$ is the ground states and f runs on the excited states of the Hamiltonian. The sum can be extended to the ground state, since for any non-degenerate state $\langle g|\,\hat{\vec{m}}\,|g\rangle = 0$. The eigenstates of an Hamiltonian constitute a complete and orthonormal basis, so that, applying closure, eq. 1 becomes:

$$\sum_f R_{gf} = \mathrm{Im}(\langle g|\,\hat{\vec{\mu}} \cdot \hat{\vec{m}}\,|g\rangle) = 0$$

The above expression vanishes since the diagonal element of the Hermitian operator $\hat{\vec{\mu}} \cdot \hat{\vec{m}}$) is real.

2 TD-DFT calculations

We run TD-DFT calculations for (a) the twisted chromoforic unit (geometry from the crystal structure, see main text) and (b) the planar chromophoric unit (optimized in gas phase with a DFT calculation, B3LYP/6-31G(d)). Results obtained with four different DFT functionals: B3LYP, PBE0, CAM-B3LYP and M062X (6-31G(d) basis set in all cases) are reported in Tabs. S1 and S2. The oscillator strengts, the amplitude of electric and magnetic transition dipole moments, and the $\mu - m$ angles are very similar for all functionals. Significant variations are observed for the energy of the second excited state. However, this dark state is located at much higher energy than the lowest excited state and is therefore irrelevant in the description of the low-energy spectral properties. [1–3]

In both geometries, the first excitation at ~ 3 eV is a bright HOMO-LUMO transition (Fig. S1), with a transition electric dipole moment $\mu \sim 13$ D, polarized along the polymethinic bridge, and a sizeable transition magnetic dipole moment $m \sim 1.4$ and 1.5 atomic units, for the twisted and planar geometries respectively. The magnetic dipole moment is perpendicular to the cyanine π-conjugated system for the planar non-chiral core, resulting in a vanishing rotational strength. In the twisted chiral geometry instead, the the magnetic and electric dipoles form a 89.5° angle (Tab. S1 and lower panel of Fig. 3).

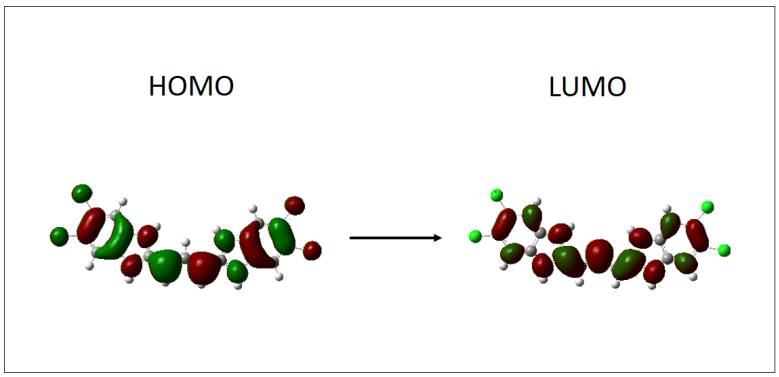

Figure S1: Orbitals involved in the lowest lying (HOMO-LUMO) transition for the planar chromophoric core of C8O3. Orbital contribution does not significantly vary for the twisted C8O3.

	B3LYP	**PBE0**	**CAM-B3LYP**	**M062X**
E_1 (eV)	2.88	2.95	3.06	3.02
E_2 (eV)	3.85	4.04	4.60	4.60
f_1	2.0	2.1	2.1	2.1
f_2	0.0	0.0	0.0	0.0
R_1 (a.u.)	12.95	13.98	17.43	18.76
R_2 (a.u.)	0.0	0.0	0.0	0.0
m_1 (a.u.)	1.4	1.4	1.4	1.4
μ_1 (D)	13	13	13	13
$\mu_1 - m_1$ angle (°)	89.5	89.5	89.4	89.4

Table S1: TD-DFT results obtained with different functionals for the C803 twisted chromophoric core. The 1 and 2 subscripts refer to the first and second excited state, respectively. E is the transition energy, f and R the oscillator strength and rotational strength, respectively.

	B3LYP	**PBE0**	**CAM-B3LYP**	**M062X**
E_1 (eV)	2.87	2.93	3.04	3.00
E_2 (eV)	3.85	4.04	4.60	4.60
f_1	2.0	2.1	2.1	2.0
f_2	0.0	0.0	0.0	0.0
μ_1 (D)	13	13	13	13
m_1 (a.u.)	1.5	1.5	1.5	1.6
$\mu_1 - m_1$ angle (°)	90	90	90	90

Table S2: TD-DFT results obtained with different functionals for the C803 planar chromophoric core. The 1 and 2 subscripts refer to the first and second excited state, respectively. E is the transition energy and f the oscillator strength. Rotational strengths (not shown) vanish for this non-chiral structure.

3 Extraction of electric transition dipole moment from the experimental absorption spectrum

The integrated area below the molar extinction coefficient curve plotted against wavenumbers (in cm^{-1}) is proportional to the oscillator strength F_{kg} relative to the transition from the ground state to the k-th excited state[4]:

$$F_{kg} = 4.33 \times 10^{-9} \int_{band} \epsilon(\tilde{\nu}) d\tilde{\nu}$$

F_{kg} is in turn related to the squared electric transition dipole moment:

$$F_{kg} = \frac{2 m_e \omega_{kg}}{3 \hbar e^2} |\mu_{kg}|^2$$

where m_e is the electron mass and ω_{kg} is the frequency relative to the transition from the ground state to the k-th excited state.

4 Absorption and CD spectra of planar C8O3

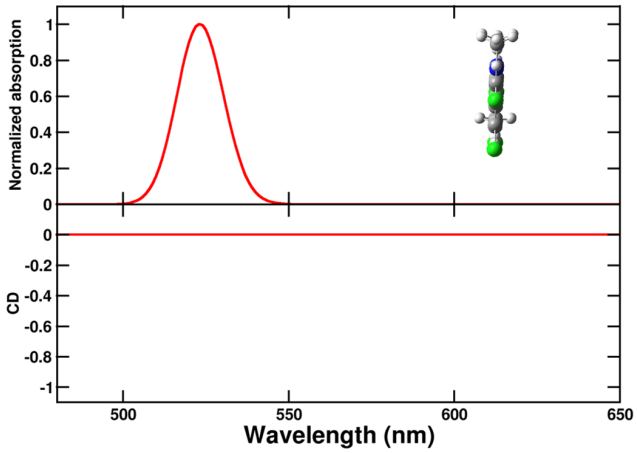

Figure S2: Normalized absorption (upper panel) and circular dichroism (CD, lower panel) spectra of the planar C8O3 chromophoric core. Spectra are broadened using a gaussian bandwidth $\sigma = 0.045$ eV, according to Eq. (S7).

5 Tubes geometry

Due to the cylindrical shape of the tubes,[5,6] it is convenient to work with cylindrical coordinates. They define the position of the center of mass of each molecule in terms of the radial distance from the tube axis, ρ; the angle θ, which defines the position of the molecule in the XY plane perpendicular to the tube axis Z; the quota z, which is the position of the molecule along the tube axis. This set of coordinates is related to cartesian coordinates x, y, z by simple transformations as reported in Eqs. 1:

$$\begin{aligned} x &= \rho cos(\theta) \\ y &= \rho sin(\theta) \\ z &= z \end{aligned} \tag{1}$$

The center of mass of each cyanine is located in a point $\vec{r}$ on the surface of a tube of diameter d, so that $\rho = \frac{d}{2}$. The relevant cylindrical coordinates are:

$$\vec{r} = (\frac{d}{2}cos(\theta), \frac{d}{2}sin(\theta), z) \tag{2}$$

Cyanines are arranged in rings with the angular distance between two adjacent cyanines in each ring defined by θ'. Rings are stacked along the z axis with spacing s and are mutually rotated around the z axis by a twist angle ϕ. Accordingly, setting the coordinates of the first cyanine as $(\frac{d}{2}, \frac{d}{2}, 0)$, the coordinates of the i-th cyanine in the j-th ring, $\vec{r}_{i,j}$ are:

$$\vec{r}_{i,j} = \Big(\frac{d}{2}cos\big((i-1)\theta^{'} + (j-1)\phi\big), \frac{d}{2}sin\big((i-1)\theta^{'} + (j-1)\phi\big), (j-1)s\Big) \quad (3)$$

The electric transition dipole moment, $\vec{\mu}$, oriented along the cyanine polymethine bridge, is tangent to the cylinder wall, forming a β angle with the tube axis. In order to ensure orthogonality with the radius, $\vec{\mu}$ should lie along one of the unit vectors $(-\sin(\theta)\sin(\beta), \cos(\theta)\sin(\beta), \cos(\beta))$, with β determining its component along the tube axis. This guarantees the scalar product with the radius to be null, implying the dipole moment is tangent to the surface.

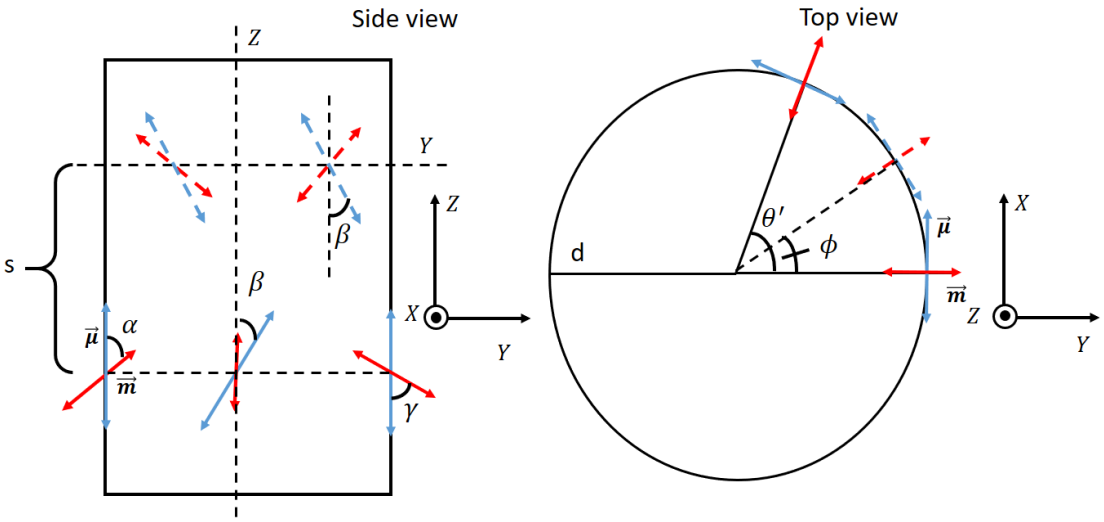

Figure S3: Side (left panel) and top (right panel) views of the tubular aggregate geometry, illustrating the various parameters. The electric and magnetic transition dipole moments are represented as blue and red double-headed arrows, respectively. The dipole moments of the upper row are represented as dashed lines in order to distinguish the rows in the top view.

In the "herringbone-like" tube geometry the electric dipole moments of the cyanines in the j-th circle form a β angle with positive direction of the tube axis, Z, while the electric dipole moments of cyanines in the $(j+1)$-th circle form the same angle with the opposite direction of the tube axis, and the ϕ rotation between stacked circles is equal to $\frac{\theta^{'}}{2}$.

The direction of the magnetic transition dipole moment $\vec{m}$ is $(cos(\theta)sin(\gamma), sin(\theta)sin(\gamma), cos(\gamma))$, so that the scalar product between mag-

netic and electric transition dipole moments of each cyanine is proportional to $cos(\beta)cos(\gamma)$ and the angle between them, α, is $\alpha = arccos(cos(\beta)cos(\gamma))$. It should be noticed that the projections of $\vec{\mu}$ and $\vec{m}$ on the xy plane are orthogonal, thus ensuring the molecular chiroptical response is coupled to longitudinal modes only. We keep the α value close to that obtained by TD-DFT results (Tab. S1). All geometrical parameters employed to build the single tube are reported in Tab. S3 and illustrated in Fig. S3.

Parameter	Value
d	20 Å
$\theta^{'}$	30°
β	50°
γ	90.8°
α	90.5°
ϕ	15°
s	14 Å
N	240

Table S3: Geometrical parameters employed for C8O3 calculations.

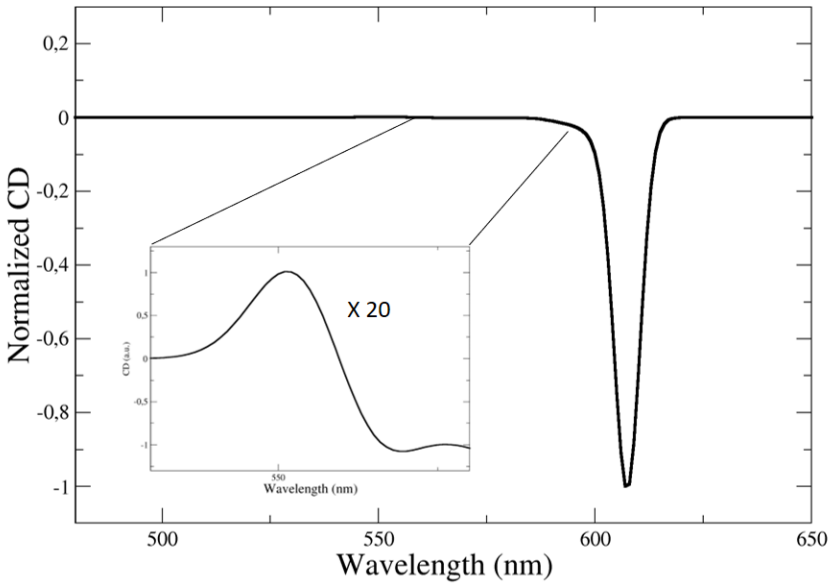

Figure S4: CD spectra of a single tube calculated for a distorted herringbone with ϕ=23°. The $\mu-\mu$ coupling contribution which appears at lower wavelengths is amplified in the inset.

6 Exciton model and calculation of spectra

The aggregate Hamiltonian is written on the basis formed by the states $|n,i\rangle$, defined as the states where all molecules are in the ground state, but the i-th molecule in the n-th unit cell that is in the excited state. The exciton approximation neglects interactions between states having different energies,[7–9] so that for an aggregate of N identical molecules the $N \times N$ Hamiltonian matrix is:

$$\hat{H} = \begin{bmatrix} E_0 & ... & ... & ... & ... & ... \\ ... & E_0 & ... & J(n,i;m,j) & ... & ... \\ ... & ... & E_0 & ... & ... & ... \\ ... & J(m,j;n,i) & ... & E_0 & ... & ... \\ ... & ... & ... & ... & E_0 & ... \\ ... & ... & ... & ... & ... & E_0 \end{bmatrix} \tag{4}$$

where E_0 is the monomer transition energy and the interaction energy $J(n,i;m,j) = \langle n,i|\,\hat{H}\,|m,j\rangle$ is expressed in the dipolar approximation as follows:

$$J(n,i;m,j) = \frac{1}{4\pi\epsilon_0\eta^2}\frac{\vec{\mu}_{n,i}\cdot\vec{\mu}_{m,j} - 3(\vec{\mu}_{n,i}\cdot\vec{n}_{m,j;n,i})(\vec{\mu}_{m,j}\cdot\vec{n}_{m,j;n,i})}{r^3_{m,j;n,i}} \tag{5}$$

where ϵ_0 is the vacuum dielectric constant, η is the medium refractive index at optical frequencies, $\vec{\mu}_{n,i}$ is the electric transition dipole moment vector of molecule i in the n unit cell, and $\vec{n}_{m,j;n,i}$ is the unit vector defining the distance between molecules i and j in unit cells n and m, its length being $r_{m,j;n,i}$. We set $\eta = 1.6$, as relevant for organic films[10]. The amplitude of the electric transition dipole moment is 9.6 D and the monomer transition energy E_0 is fixed at 2.37 eV (523 nm).

The diagonalization of the Hamiltonian in Eq. 4 gives the eigenstates as a linear combination of the basis states:

$$|\Psi_k\rangle = \sum_{i,n} c_{n,i;k}\,|n,i\rangle$$

with $c_{n,i;k} = \langle n,i|\Psi_k\rangle$.

The electric transition dipole moment from the ground state $|G\rangle$ (the state where all molecules are in the ground state) to $|\Psi_k\rangle$ reads:

$$\langle G|\,\hat{\vec{\mu}}\,|\Psi_k\rangle = \sum_{n,i} c_{n,i;k}\vec{\mu}_{n,i} \tag{6}$$

The absorption spectrum is calculated assigning a Gaussian lineshape of appropriate bandwidth σ to each transition:

$$\epsilon(\omega) = \frac{N_A 4\pi\omega}{3\ln(10)\hbar c}10^{-3}\sum_k \frac{|\,\langle G|\,\hat{\vec{\mu}}\,|\Psi_k\rangle\,|^2 e^{-\frac{(\omega-\omega_k)^2}{2\sigma^2}}}{\sigma\sqrt{2\pi}} \tag{7}$$

where ω_k is the frequency of the transition from the ground state to $|\Psi_k\rangle$, c is the light velocity in vacuum and N_A is Avogadro's number.

As the tube axis is aligned along the Z direction (as in section 5), the longitudinal contribution to absorption can be calculated by considering the z component of the electric dipole moment operator, as:

$$\epsilon_l(\omega) = \frac{N_A 4\pi\omega}{3\ln(10)\hbar c} 10^{-3} \sum_k \frac{|\langle G|\hat{\mu}_z|\Psi_k\rangle|^2 e^{-\frac{(\omega-\omega_k)^2}{2\sigma^2}}}{\sigma\sqrt{2\pi}} \tag{8}$$

The transverse contribution to absorption can be obtained by considering the components of the electric transition dipole moments perpendicular to the z direction. In particular:

$$\epsilon_t(\omega) = \frac{N_A 4\pi\omega}{3\ln(10)\hbar c} 10^{-3} \sum_k \frac{(|\langle G|\hat{\mu}_x|\Psi_k\rangle|^2 + |\langle G|\hat{\mu}_y|\Psi_k\rangle|^2) e^{-\frac{(\omega-\omega_k)^2}{2\sigma^2}}}{\sigma\sqrt{2\pi}} \tag{9}$$

The magnetic transition dipole moment from the ground state $|G\rangle$ to $|\Psi_k\rangle$ is:

$$\langle G|\hat{\vec{m}}|\Psi_k\rangle = \sum_{n,i} c_{n,i;k}\vec{m}_{n,i} \tag{10}$$

The rotational strength associated to the $|G\rangle$ to $|\Psi_k\rangle$ transition reads:

$$R_k = \sum_{n,m,i,j} c_{n,i;k}c_{m,j;k}\Big(\frac{\omega_k}{4c}(\vec{r}_{m,j;n,i}\cdot\vec{\mu}_{m,j}\times\vec{\mu}_{n,i}) + \vec{m}_{m,j}\cdot\vec{\mu}_{n,i}\Big) \tag{11}$$

where the first term in brackets accounts for μ-μ coupling and the second for μ-m coupling and intrinsic chirality. The CD spectrum is finally calculated as [11]:

$$\Delta\epsilon(\omega) = \frac{N_A 16\pi\omega}{3\ln(10)\hbar c} 10^{-3} \sum_k \frac{R_k e^{-\frac{(\omega-\omega_k)^2}{2\sigma^2}}}{\sigma\sqrt{2\pi}} \tag{12}$$

In order to facilitate comparison with the experiment, the longitudinal mode has been assigned a bandwidth $\sigma = 0.014eV$ and the transversal mode a bandwidth $\sigma = 0.045eV$ [12].

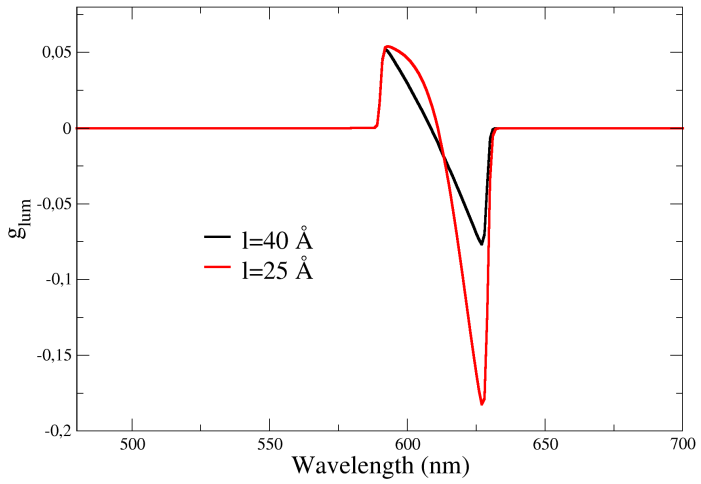

Figure S5: Calculated CPL spectra (expressed as g_{lum} vs wavelength) of C803 bundle calculated for two different intertube distance l.

References

[1] F. Terenziani, A. Painelli, C. Katan, M. Charlot and M. Blanchard-Desce, *J. Am. Chem. Soc.*, 2006, **128**, 15742–15755.

[2] F. Terenziani, O. Przhonska, S. Webster, L. Padilha, Y. Slominsky, I. Davydenko, A. Gerasov, Y. Kovtun, M. Shandura, A. Kachkovski, D. Hagan, E. Van Stryland and A. Painelli, *J. Phys. Chem. Lett.*, 2010, **1**, 1800–1804.

[3] F. Bertocchi, A. Delledonne, G. Vargas-Nadal, F. Terenziani, A. Painelli and C. Sissa, *J. Phys. Chem. C*, 2023, **127**, 10185–10196.

[4] J. Lakowicz, *Principles of Fluorescence Spectroscopy*, Springer, 2006, vol. 1.

[5] H. von Berlepsch, C. Böttcher, A. Ouart, C. Burger, S. Dähne and S. Kirstein, *J. Chem. Phys. B*, 2000, **104**, 5255–5262.

[6] S. Kirstein, H. von Berlepsch, C. Böttcher, C. Burger, A. Ouart, G. Reck and S. Dähne, *ChemPhysChem*, 2000, **1**, 146–150.

[7] Kasha, M., *Radiat. Res.*, 1964, **3**, 317–331.

[8] F. Terenziani and A. Painelli, *Phys. Rev. B*, 2003, **68**, 165405.

[9] M. Anzola and A. Painelli, *Phys. Chem. Chem. Phys.*, 2021, **23**, 8282–8291.

[10] C. Garcia, J. Correa, D. Espalin, J. Barton, R. Rumpf and R. Wicker, *Prog. Electromagn. Res. Lett.*, 2012, **34**, 75–82.

[11] F. Bertocchi, C. Sissa and A. Painelli, *Chirality*, 2023, **35**, 681–691.

[12] D. Eisele, C. Cone, E. Bloemsma, S. Vlaming, C. Kwaak, R. Silbey, M. Bawendi, J. Knoester, J. Rabe and D. Vanden Bout, *Nat. Chem.*, 2012, **4**, 655–662.